BULLETIN OF THE POLISH ACADEMY OF SCIENCES
TECHNICAL SCIENCES, Vol. 69(5), 2021, Article number: e138816
DOI: 10.24425/bpasts.2021.138816

Comparison of Electrochemical Micromachining Performance using TOPSIS, VIKOR and GRA for Magnetic field and UV rays heated Electrolyte

K.G. SARAVANAN[1], R. THANIGAIVELAN[2*], and M. SOUNDARRAJAN[2]

[1] Sona College of Technology (Autonomous), Salem-636005, Tamil Nadu, India
[2] Muthayammal Engineering College (Autonomous), Rasipuram-637408, Tamil Nadu, India

Abstract. The application of micro components in various fields such as biomedical, medical, automobile, electronics, automobile and aviation significantly improved. To manufacture the micro components, different techniques exist in the non-traditional machining process. In those techniques, electrochemical micromachining (ECMM) exhibits a unique machining nature, such as no tool wear, non-contact machining process, residual stress, and heat-affected zone. Hence, in this study, micro holes were fabricated on the copper work material. The sodium nitrate ($NaNO_3$) electrolyte is considered for the experiments. During the experiments, magnetic fields strength along with UV rays are applied to the electrolyte. The L_{18} orthogonal array (OA) experimental design is planned with electrolyte concentration (EC), machining voltage (MV), duty cycle (DC) and electrolyte temperature (ET). The optimization techniques such as similarity to ideal solution (TOPSIS), VlseKriterijumska Optimizacija I Kompromisno Resenje (VIKOR) and grey relational analysis (GRA) were employed to find the optimal parameter combinations. The entropy weight method is used to assess the weight of responses such as MR and OC. The optimal combination using TOPSIS, VIKOR and GRA methods shows the same results for the experimental runs 8, 9 and 7, and the best optimal parameter combination is 28 g/l EC, 11 V MV, 85% DC and 37°C ET. Based on the analysis of variance (ANOVA) results, electrolyte concentration plays a significant role by contributing 86% to machining performance. The second and least contributions are DC (3.86%) and ET (1.74%) respectively on the performance. Furthermore, scanning electron microscope (SEM) images analyses are carried out to understand the effect of magnetic field and heated electrolyte on the work material.

Key words: electrolyte; magnet; UV heating; TOPSIS; VIKOR; GRA.

1. INTRODUCTION

Copper is an essential metal alloy used for various applications in electronic sectors, aerospace, biomedical, medical and automobiles industries. Due to its ductile nature and crystallographic microstructure, it is difficult to machining copper in the traditional method. The high spindle speed, tool edge accuracy, chip intervention between the tool and work, temperature rise due to the friction and formation of burrs are concerns that hinder the machining accuracy significantly [1–6].To overcome these non-contact, burr-free, no residual stress and high accuracy machining methods such as ECMM are preferred for the micro holes generation on the copper work material. Various research attempts were carried out in the past decade; Ao et al. [7] tried the ethylene glycol, and sodium chloride (NaCl) mixed water-free electrolyte with ECMM for shape memory alloy. The higher ethanol concentration reduces the oxide development over the machining surface. Soundarrajan *et al*. [8] tried the hydrochloric acid mixed $NaNO_3$ electrolyte in ECMM for Al-6063 composite. They compared the results among acidic electrolytes to the non acidified electrolyte and reported that faster ion displacement in the acidic electrolyte contributes to higher MR. Pooranachandran *et al.* [9] explored the flushing of electrolytes in ECMM for machining nickel-based Inconel alloy and copper. The electrodes such as copper and brass are employed to machine the work material, and electrolyte flushing increases the removal of the passivation layer from the workpiece. Pan *et al.* [10] adopted the pressurized, hydrostatic electrolyte in ECMM to produce the micro dimples. This electrolyte enhances the uniform distribution of oxygen in the electrolyte resulting in uniform electrical conductivity. This type of electrolyte improves the accuracy of micro dimples. Baoji *et al.* [11] used magnetic field-assisted NaCl electrolyte and the stainless steel (SS) 304 material as the electrode to machining the copper. Along with this electrolyte, Iron-III chloride ($FeCl_3$) particles are mixed, and the concentration levels of the magnetic field in ECMM causes a notable improvement in machining performance. Vinothkumar *et al.* [12] attempted with oxalic acid electrolyte to study the process parameter of ECMM on SS 316L. The use of organic electrolytes like oxalic acid improves the life period of the machine. In addition, two times more MR is achieved by using the organic oxalic acid electrolyte. Rajan *et al.* [13] studied the ECMM process parameters with an induction heated $NaNO_3$ electrolyte for Al-7075 composite. The machining performances are measured in terms of MR, OC and delamination factors. The optimal parameter combination for higher MR and lower OC and DF is determined using the TOPSIS method. Thanigaivelan *et al.* [14] investi-

*e-mail: tvelan10@gmail.com

Manuscript submitted 2021-05-29, revised 2021-07-21, initially accepted for publication 2021-08-17, published in October 2021

gated the ECMM process parameters with infrared (IR) heated electrolyte for copper material. In all experiments, they kept constant electrolyte temperature at 37 ± 0.5°C in all experiments and compared those results with non-heated electrolytes. They noticed four times higher MR with IR heated electrolyte than non-heated electrolyte at the parameter combination of 25% DC, 9 V MV and 35 g/l EC. Even though high OC is found on the micro holes because of the high localization effect in the heated electrolyte. Kai Jiang *et al.* [15] suspended the boron carbide particles (B_4C) in an aqueous $NaNO_3$ electrolyte on SS-304 work material through ECMM. Electrode vibrations are applied to reduce the bubble development over the electrode. This ensures the constant current flow in the electrolyte, which enhances the removal of machined products at the machining zone. Liu *et al.* [16] blended the ethylene glycol in NaCl aqueous electrolyte for machining the titanium through the ECMM process. The results show that 25 µs pulse width, 1 μms^{-1} feeding rate and 40 V produces the best MR on the titanium work material. Also, they mentioned that the oxide layer formation on titanium work material hinders the machining performance significantly. Anup Malik *et al.* [17] employed laser in the electrolyte to study the performance of electrochemical machining (ECM) on Inconel-718 alloy. They compared the results of ECM using laser-assisted electrolytes with non-laser assisted electrolytes. The laser-assisted electrolyte produces better MR and reduces the taper angle generation significantly. The use of laser increases the electrolyte temperature, which produces 29% higher MR than the plain electrolyte. Zhang *et al.* [18] adopted the semi-solid electrolyte to fabricate the high aspect ratio micro tool using the ECMM process. The use of semi-solid electrolytes shows a significant contribution compared to liquid electrolytes. Alistair *et al.* [19] attempted the machining with various electrolytes such as NaCl, sodium fluoride and sodium bromide. NaCl and sodium fluoride electrolytes hinder the oxide layer passivations on titanium alloy, which reduces the OC. Sekar *et al.* [20] mixed the copper nanopowders in NaCl electrolyte to study the performance of ECM for die steel. The use of copper nanopowders mixed electrolyte increases the machining rate due to hydrogen bubbles collision around the tool electrode. Also, uniform current flow in the inter-electrode gap (IEG) causes the lowest surface roughness of 1.39 µm. Hence from the above works of literature, it is evident that electrolyte performance in ECMM plays a vital role in machining accuracy. Moreover, the optimization of ECMMparameters is essential for the commercialization of technology. Mohanty *et al*. [21] tried the fuzzy TOPSIS method, Singh *et al*. [22] have adapted the firefly algorithm, Mehrvar *et al*. [23] used the RSM and differential estimation algorithm, Mythreyi *et al*. [24] used grey relational technique to evaluate the optimal process parameter combination. Hence, the literature of the previous work clears that the researches on different electrolytes and performance of ECMM were investigated and very few studies are carried out related to heated electrolytes and their optimizations. In literature, researchers have carried out experiments with the electrolyte heating techniques such as infrared, induction, ultrasonic vibrations and UV rays [13, 14, 25, 26]. Among those methods, UV rays heated electrolyte shows the significant improvement in MR. The use of UV rays heating avoids the heating of ECMM subsystems, and rapid heating of electrolytes is achieved. Therefore, in this paper, an amalgamation of UV rays heating and the magnetic field strength is applied in the electrolyte [27]. In ECMM, cations will move towards the cathode, and anions will move towards the workpiece. The electric force in the electrolyte drives the movement of ions in a straight path. According to the Lorentz force, when the magnetic field is applied in the electrolyte, it owes extra energy force and electric force. Hence in this research, the ECMM process parameters are optimized using TOPSIS, VIKOR and GRA methods considering the UV rays heating and magnetic field. The weight of the output responses is calculated using the entropy method. The Taguchi L_{18} orthogonal array (OA) experimental design is used for conducting the experiments along with input parameters such as EC, MV, DC and ET for higher MR and lower OC.

2. EXPERIMENTAL SETUP

ECMM system has been fabricated indigenously to carry out the experiments. The setup includes different parts such as a power supply system, tool feeding system, and electrolyte supply system, as shown in Fig. 1. The electrolyte tank is made of acrylic material, and a filter is attached to remove the reaction products. When the microprocessor sends the pulse to the stepper motor, it creates a linear movement of 4 µm. Copper plate of thickness 800 µm is considered work material, and stainless steel electrode of diameter 500 µm is insulated with epoxy bonding resin. Sodium nitrate ($NaNO_3$) salt is used as an electrolyte with different levels of concentration. The sodium nitrate brine solution is prepared for various concentrations with distilled water. The brine solution is prepared by mixing the weighed sodium nitrate salts in one liter of distilled water. The solution is mixed thoroughly with a magnetic stirrer. For each experiment, fresh electrolytes are prepared and used.

Four factors at three levels, as shown in Table 1, attribute for degrees of freedom (eight), and hence the OA of more than 8 has to be considered. The duty cycle is defined as the ratio of pulse on time to the total time for a fixed frequency. L_{18} OA is employed to carry out the experiments as presented in Table 2. The electrolyte is heated through a commercially

Fig. 1. Electrochemical micromachining setup

Table 1
Machining parameters and their levels

Symbol	Machining Parameters	Level 1	Level 2	Level 3
EC	Electrolyte Concentration [g/l]	20	25	30
MV	Machining Voltage [V]	7	8	9
DC	Duty Cycle [%]	45	55	65
ET	Electrolyte Temperature [°C]	32	34	36

Table 2
Design of experiments L_{18} OA

Ex. No	EC	MV	DC	ET
1	24	9	70	35
2	24	11	55	37
3	24	13	85	39
4	26	9	70	37
5	26	11	55	39
6	26	13	85	35
7	28	9	55	35
8	28	11	85	37
9	28	13	70	39
10	24	9	85	39
11	24	11	70	35
12	24	13	55	37
13	26	9	55	39
14	26	11	85	35
15	26	13	70	37
16	28	9	85	37
17	28	11	70	39
18	28	13	55	35

available 70 W Ultraviolet (UV) heating light. The magnets arrangement in the electrolyte tank is shown in Fig. 2. The wall of the electrolyte tank is affixed by permanent magnets, which are used to swirl the electrolyte molecules. The heated electrolyte coupled with magnets energies the electrolyte molecules to the next level, increasing the ions' movement. The digital thermometer was used to measure electrolyte temperature. In ECMM, the machining voltage (≤10 V) hence in micromachining, slight change in voltage and temperature will have a significant effect.

3. MULTI-OBJECTIVE OPTIMIZATION TECHNIQUES

3.1. Entropy Method

The entropy method is an improved method for determining the weight of the evaluating indicators that were applied in TOPSIS, VIKOR and GRA techniques. The Entropy weight method [25] comprises the following steps:

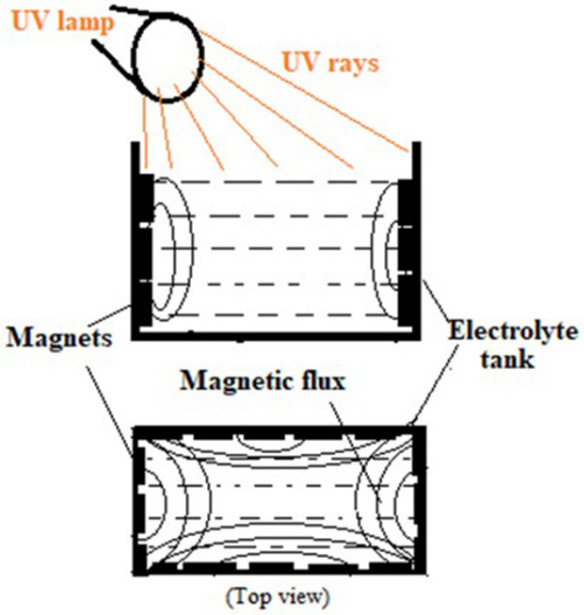

Fig. 2. Views of electrolyte tank and magnets arrangement

Step 1: The responses are arranged in the decision matrix as per Eq. (1), which contains 'n' attributes and 'm' alternatives for decision.

$$Z = \begin{bmatrix} Z_{11} & Z_{12} & Z_{13} & \cdots & \cdots & Z_{1n} \\ Z_{21} & Z_{22} & Z_{23} & \cdots & \cdots & Z_{2n} \\ Z_{31} & Z_{32} & Z_{33} & \cdots & \cdots & Z_{3n} \\ \vdots & \vdots & \vdots & \ddots & \ddots & \vdots \\ \vdots & \vdots & \vdots & \ddots & \ddots & \vdots \\ Z_{m1} & Z_{m2} & Z_{m3} & \cdots & \cdots & Z_{mn} \end{bmatrix}, \quad (1)$$

where Z_{ij} (i = 1, 2, …, m; j = 1, 2, …, n) signify the value of the i-th evaluation alternative in the j-th indicator, and Z_j (j = 1, 2, …, n) indicate the column vector data of all evaluation alternatives of the j-th indicator.

Step 2: The responses of matrix values are normalized using Eq. (2).

$$K_{ij} = \frac{P_{ij}}{\sqrt{\sum_{i=1}^{m} k_{ij}^2}} \qquad j = 1, 2, \ldots, n, \quad (2)$$

where K_{ij} is a normalized value between the interval [0, 1] for i^{th} alternative and j^{th} attribute.

Step 3: The Entropy value F_j is calculated using Eq. (3).

$$F_j = -k \sum_{i=1}^{m} K_{ij} \ln\left(K_{ij}\right) \qquad j = 1, 2, \ldots, n, \quad (3)$$

where $k = \frac{1}{\ln m}$ is non-negative constant, m is the no of alternatives.

Step 4: The degree of divergence can be calculated using Eq. (4).

$$D_j = 1 - F_j. \tag{4}$$

Step 5: The result of this weight of j th criteria could be calculated using Eq. (5).

$$W_{ij} = \frac{D_j}{\sum_{j=1}^{n} D_j} \tag{5}$$

3.2. TOPSIS Method

TOPSIS is the most power full tool to isolate the proper parametric combination from the limited experimental combination. The steps used in this method are listed below [25, 28]:

Step 1: The decision matrix and normalizing of data has been carried out using Eq. (1, 2)

Step 2: The weight of every attribute were assumed to be W_j (j = 1, 2, …, n). The normalized weighted decision matrix M_{ij} is obtained by Eq. (5).

Step 3: The positive (best) ideal solution is evaluated by Eq. (6), and the negative ideal solution is obtained by Eq. (7).

$$Y^+ = \left\{\left(\sum_i^{max} M_{ij} \,|\, j \in J|\right)\right\}, \left\{\left(\sum_i^{min} |\, j \in J|\ i = 1, 2, \ldots, m\right)\right\} = \left\{x_1^+, x_2^+, x_3^+, \ldots, x_n^+\right\}, \tag{6}$$

$$Y^- = \left\{\left(\sum_i^{min} M_{ij} \,|\, j \in J|\right)\right\}, \left\{\left(\sum_i^{max} |\, j \in J|\ i = 1, 2, \ldots, m\right)\right\} = \left\{x_1^-, x_2^-, x_3^-, \ldots, x_n^-\right\} \tag{7}$$

Step 4: The separation between each alternative is calculated from the 'ideal' solution is given by Eq. (8).

$$P_i^+ = \sqrt{\sum_{j=1}^{n} \left(M_{ij} - x_j^+\right)^2}, \quad i = 1, 2, \ldots, m \tag{8}$$

The separation of alternatives form the 'negative ideal' solution is evaluated using Eq. (9).

$$P_i^- = \sqrt{\sum_{j=1}^{n} \left(M_{ij} - x_j^-\right)^2}, \quad i = 1, 2, \ldots, m \tag{9}$$

Step 5: Equation (8) is used to find the relative proximity of the different alternatives to the ideal solution.

$$R_i = \frac{P_i^-}{P_i^+ + P_i^-} \qquad i = 1, 2, \ldots, m \tag{10}$$

Step 6: The preference values (R_i) are ranked in descending order to find the optimal parameters combination.

3.3. VIKOR Method

VIKOR is a multi criteria optimization method to categorize the suitable parameter combination within the experiments. The following steps are followed for the VIKOR method [29]:

Step 1: The normalized values are obtained from the Eqs. (1) and (2). In this step, the responses assigned negative sign for minimization and positive sign assigned for maximization.

Step 2: The maximum $(n_{ij})_{max}$ and minimum $(n)_{min}$ values are taken from the decision matrix for all criteria's. Therefore Q_i and R_i values were calculated using Eq. (11) and (12).

$$Q_i = \sum_{j=1}^{n} W_j \left[(n_{ij})_{max} - (n_{ij})\right] \Big/ \left[(n)_{max} - (n_{ij})_{min}\right] \tag{11}$$

$$R_i = \text{Max}^n \text{of} \left\{\left[W_j (n)_{max} - (n_{ij})\right] \Big/ \left[(n)_{max} - (n_{ij})_{min}\right]\right\} \quad j = 1, 2, \ldots, n, \tag{12}$$

where W_j is the weight value which has been calculated based entropy weighted method using Eqs. (1)–(5).

Step 3: The U_i values are calculated using Q_i and R_i by Eq. (13).

$$U_i = w\left((Q_i - Q_{i-min}) / (Q_{i-max} - Q_{i-min})\right) + + (1-w)\left((R_i - R_{i-min}) / (R_{i-max} - R_{i-min})\right), \tag{13}$$

where Q_{i-max} denotes the highest value of Q_i, and Q_{i-min} denotes the least value of Q_i. As well as R_{i-max} is the highest value of R_i and R_{i-min} is the lowest value of R_i. Generally, w is taken from Eq. (5).

Step 4: Q_i, R_i and U_i values are arranged in ascending order to rank the final criteria's. According to the T_i value, the best solution is obtained, and the least value of T_i is considered the best value, which is ranked as one.

3.4. GRA Method

In GRA, the response values of the various entity must be transformed into the dimensionless value. The values are normalized in the range of zero to one [26].

Step 1: The values are normalized using the following Eqs. (14) and (15).

$$Y_i^*(P) = \frac{X_i(Q) - \text{Min } X_i(Q)}{\text{Max } X_i(Q) - \text{Min } X_i(Q)} \tag{14}$$

For (i = 1, 2 … m, P = 1, 2 … n)

$$y_i^*(P) = \frac{\text{Max } x_i(Q) - x_i(Q)}{\text{Max } x_i(Q) - \text{Min } x_i(Q)} \tag{15}$$

For (i = 1, 2 … m, Q = 1, 2 … n)

where m is the total number of experiments, n is the total number of observed data.

Step 2: The normalized values are used in Eq. (16) to calculate the grey relational coefficient (GRC).

$$\beta_i(P) = \frac{\Delta_{Min} + \zeta\Delta_{Max}}{\Delta_{oi}(P) + \zeta\Delta_{Max}} \quad (16)$$

Here $\Delta_{oi}(P)$ deviation sequence is obtained form reference sequence $X_0^*(P)$ and comparability sequence $X_i^*(P)$. The range $0 \leq \xi \leq 1$ is used for the distinguishing coefficient β.

Step 3: The grey relational grades (GRG) are calculated using averaging the GRC by using Eq. (17).

$$\lambda_i = \frac{1}{n}\sum_{P=1}^{n} W_{ij}\beta_i(P) \quad (17)$$

A GRG (λ_i) is an entropy weighted (W_{ij}) value that helps find the highest rank.

4. RESULT AND DISCUSSION

4.1. Influences of Input parameters on MR

The machining performance of ECMM is studied with the help of Fig. 3. The mean values of MR are considered for plotting the graph against the process parameters. The graph depicts that higher-level process parameters produce the higher MR. Also, the MR increases consistently with parameters levels. The highest and least MR are obtained at parameter combinations of 13 V MV and 24 g/l EC, respectively.

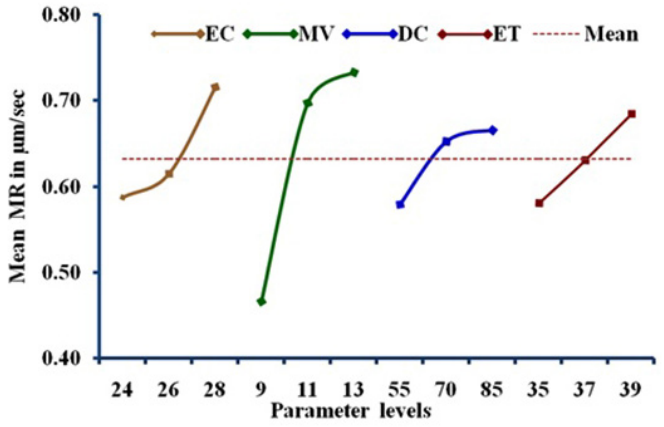

Fig. 3. Influences of process parameters on mean MR

Moreover, the highest MR, i. e. 0.733 µm/sec, is 35% higher than the normal UV heated electrolyte, which is claimed in literature [26]. Based on the literature, UV heated electrolyte triggers its molecules to move faster due to the energy transformation. In addition, the use of a magnetic field provides extra energy for ions movement. Hence, it is obvious that trigged ions in an electrolyte swirl around the tank improve the current flowability [27]. The increased momentum of the electrolyte leads to higher MR at different parameters levels. Also, the magnetic field application in the UV rays heated electrolyte multiples the MR with respect to all process parameters.

4.2. Influences of Input parameters on OC

Figure 4 represents the influences of input process parameters on OC using UV rays heated, and magnetic field applied electrolyte. According to the graph, an increase in EC increases the OC; with an increase in EC, the current conductivity increase. This attributes more reaction products that interrupt the Inter electrode gap, developing short circuits and stray current effects.

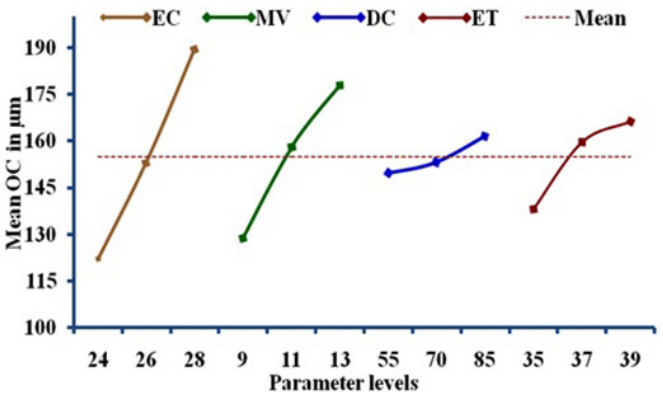

Fig. 4. Influences of process parameters on mean OC

This causes a higher OC on the work material. Moreover, higher OC is obtained in all higher process parameters due to the addition of the magnetic field effect and UV heat to the electrolyte. The SEM images of micro-holes are shown in Figs. 5 and 6 for the 1st and 2nd optimal combination, respec-

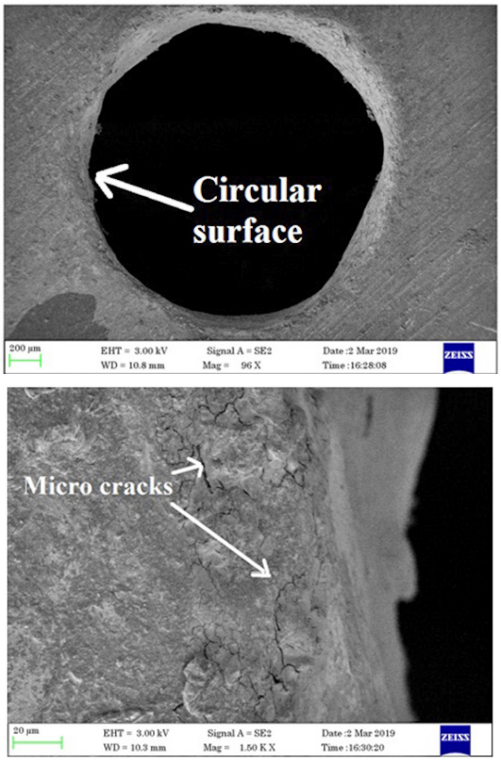

Fig. 5. SEM image of 1st optimal combination

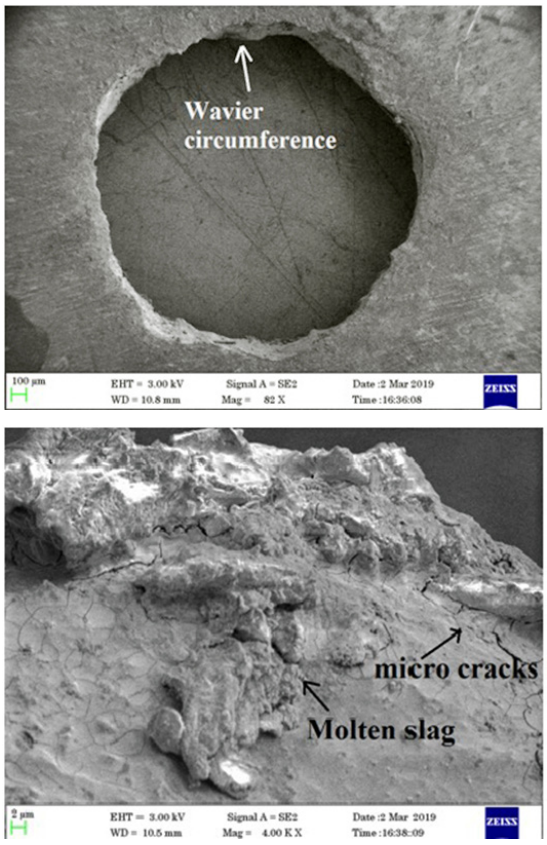

Fig. 6. SEM image of 2nd optimal combination

tively. The slight micro-cracks formations were found on the circumference of the micro-hole due to the heating of the electrolyte. The lowest and highest OC are obtained at 24 g/l and 28 g/l EC, respectively. The addition of a magnetic field in the UV heated electrolyte plays a vital role in generating higher OC. A magnetic field induces the electrolyte molecules' repulsion movement, which pushes out the machined products from the machining zone [29].

4.3. Assessment of optimal combination using TOPSIS

The outcome responses such as MR and OC using UV heated and magnetic field-assisted electrolyte were optimized using TOPSIS. The experimental results find the preference values (R_i) from the Eqs. (6)–(10). The entropy weight method estimates the weights of output responses using Eqs. (1)–(5). The weight of responses for MR and OC are 0.4987 and 0.5012, respectively. Table 3 presents the normalized values of MR and OC.

Taguchi and TOPSIS methods are combined to convert the multi-objective optimization into single-objective optimization. Thereby R_i values are obtained and ranked. The highest R_i value is considered the best optimal solution, and the highest rank is selected as the best optimal experiment. Therefore, Table 4 that the 8th experimental run (0.9052) was preferred as the 1st optimal parametric solution for machining performance for its higher R_i value. The experimental runs 9 (0.8587) and 7 (0.7583) claim the 2nd and 3rd optimal

Table 3
Normilzed responses values

Ex. No	Output Responses		Normalized Responses	
	MR (μm/sec)	OC (μm)	MR	OC
1	0.4530	154.82	0.1632	0.2290
2	0.5812	217.81	0.2094	0.3221
3	0.7262	211.43	0.2616	0.3127
4	0.3839	133.20	0.1383	0.1970
5	0.6706	120.42	0.2416	0.1781
6	0.7717	200.63	0.2780	0.2967
7	0.6806	114.61	0.2452	0.1695
8	0.8092	117.22	0.2915	0.1734
9	0.7692	117.59	0.2771	0.1739
10	0.3813	153.61	0.1374	0.2272
11	0.8601	194.61	0.3098	0.2878
12	0.5222	202.85	0.1881	0.3000
13	0.2752	106.65	0.0991	0.1577
14	0.6017	177.54	0.2168	0.2626
15	0.8651	178.48	0.3116	0.2640
16	0.6262	108.92	0.2256	0.1611
17	0.6643	120.23	0.2393	0.1778
18	0.7451	155.64	0.2684	0.2302

Table 4
TOPSIS ranking for preference values

Ex. No	P_i+	P_i-	The TOPIS preference value (R_i)	Rank
1	0.0822	0.0566	0.4077	15
2	0.0969	0.0550	0.3620	16
3	0.0816	0.0812	0.4987	11
4	0.0887	0.0657	0.4256	14
5	0.0364	0.1013	0.7356	4
6	0.0717	0.0901	0.5570	10
7	0.0337	0.1056	0.7583	3
8	0.0127	0.1215	0.9052	1
9	0.0190	0.1157	0.8587	2
10	0.0936	0.0513	0.3538	17
11	0.0652	0.1065	0.6202	9
12	0.0942	0.0457	0.3268	18
13	0.1060	0.0824	0.4374	13
14	0.0707	0.0658	0.4821	12
15	0.0533	0.1099	0.6737	8
16	0.0430	0.1024	0.7046	6
17	0.0374	0.1006	0.7288	5
18	0.0422	0.0962	0.6949	7

solutions. Hence the optimal parameter solution is found to be that 28 g/l EC, 11 V MV, 85% DC and 37°C ET using the TOPSIS method.

4.4. ANOVA for TOPSIS (R_i)

ANOVA is one of the prominent methods to find the significant process parameter. The R_i values are analyzed statistically using the ANOVA method. The results of the F-test are used to assess the significant factor for better machining performance.

Table 5 shows that the EC plays a major role in machining performance, which is 80.12% among the input factors. The MV contributes 10.56% to the machining performance, the second-highest contribution in performance measures. Table 6 presents the mean response value, which is obtained using R_i values. It shows that EC, MV and DC contribute a significant role in performance.

Table 5
ANOVA table for TOPSIS

Symbol	DF	SS	MS	F	% contribution
EC	2	0.3708	0.1854	14.31	80.12
MV	2	0.0488	0.0244	1.89	10.56
DC	2	0.0133	0.0066	0.51	2.88
ET	2	0.0038	0.0019	0.15	0.84
Error	9	0.1166	0.0129	1.00	5.60
Total	**17**	**0.5535**	**0.0325**	**17.86**	**100**

Table 6
Main effects table for TOPSIS

Machining factors symbol	Mean values of TOPSIS preference values			
	Level I	Level II	Level III	Delta
EC	0.4282	0.5519	0.7751*	0.3469
MV	0.5146	0.6390*	0.6016	0.1244
DC	0.5836	0.5525	0.6191*	0.0355
ET	0.5867	0.6022*	0.5663	0.0204

*Optimal Parametric Combination by TOPSIS: 28 g/l, 11 V, 55% and 39°C

4.5. Assessment of optimal combination using VIKOR

The VIKOR method has been used to calculate the optimal parameter combination for better machining performances of ECMM. The weights for the responses are obtained through the Entropy method.

The multi-attribute responses are converted into a single objective value using Eqs. (11)–(13). Table 7 presents the VIKOR values and their ranking order. These values are ranked as uppermost is the last and least is the first. Therefore, the lowest VIKOR value is considered the optimal process parameter solution attained in the 8th experimental run. Hence the 8th experiment parameter combination is 28 g/l EC, 11 V MV, 85% DC and 37°C ET. Using the VIKOR method, the best optimal parameter combination is obtained for these experiments. Furthermore, the 9th and 7th experimental runs are the 2nd and 3rd optimal parameter combinations found using the VIKOR method.

Table 7
Ranking of VIKOR values

Ex. No	P_i	Q_i	VIKOR (U_i)	Rank
1	0.5656	0.6554	0.7479	14
2	0.7413	0.8010	1.0000	18
3	0.5899	0.6762	0.7833	15
4	0.5265	0.6216	0.6907	12
5	0.2265	0.3326	0.2280	5
6	0.5028	0.6007	0.6556	11
7	0.1919	0.2941	0.1705	3
8	0.0949	0.1745	0.0000	1
9	0.1304	0.2209	0.0645	2
10	0.6208	0.7023	0.8280	16
11	0.4009	0.5078	0.5027	9
12	0.7237	0.7869	0.9752	17
13	0.4987	0.5971	0.6496	10
14	0.5424	0.6354	0.7140	13
15	0.3239	0.4336	0.3839	8
16	0.2122	0.3169	0.2043	4
17	0.2309	0.3374	0.2353	6
18	0.3224	0.4321	0.3815	7

4.6 ANOVA for VIKOR (U_i)

The effect of machining process parameters on MR and OC are statically analyzed using the ANOVA method (Table 8). In this, VIKOR values are considered to find the impact of parameters on machining performances. The EC plays a major role, about 86% on machining performance based on the ANOVA results. The second and most negligible contributions are DC (3.86%) and ET (1.74%), respectively. In addition, mean VIKOR values construct the main effect table, which is present in Table 9. This value correlates with the optimal combinations obtained using VIKOR (28 g/l EC, 11 V MV, 85% DC and 37° ET).

Table 8
ANOVA for VIKOR values

Symbol	DF	SS	MS	F	% contribution
EC	2	1.207	0.604	16.05	86.51
MV	2	0.039	0.019	0.51	2.76
DC	2	0.054	0.027	0.72	3.86
ET	2	0.021	0.010	0.27	1.47
Error	9	0.339	0.038		5.39
Total	**17**	**1.659**	**0.098**		**100.00**

Table 9
Main effect table for VIKOR values

Machining factors symbol	S/N ratio for VIKOR			
	Level I	Level II	Level III	Delta
EC	0.1760	0.5536	0.8062*	0.6302
MV	0.5485	0.4467*	0.5407	0.1019
DC	0.4375	0.5675	0.5309*	0.0934
ET	0.5287	0.5424*	0.4648	0.0137

*Optimal parameter solution using VIKOR: 28 g/l EC, 11 V MV, 85% DC and 37° ET

4.7. Assessment of optimal combination using GRA

The GRA is calculated using the Eqs. (14) to (17). Normalization of the data was carried out using Eqs. (14) and (15). These normalized values are considered to calculate the GRC, which is present in Table 10. The GRC values are used for the calculation of GRG, in addition to entropy weights. The weighted GRG values are ranked to assess the optimal parameter combination. The highest GRG values are considered as the best optimal solution with rank one. The experimental run 8 shows the highest GRG value, which is ranked as 1st optimal parameter combination. The experimental runs 9th and 7th show the next best experimental combinations. Based on GRA, parameter combination, i.e., 28 g/l EC, 11 V MV, 85% DC, and 37°C ET, is the best parameter solution for better machining performance.

Table 10
Ranking of VIKOR values

Ex. No	GRC		Weighted – GRC		GRG	Rank
	MR	OC	MR	OC		
1	0.588	0.697	0.293	0.349	0.321	15
2	0.675	0.500	0.336	0.250	0.293	17
3	0.809	0.514	0.403	0.258	0.330	13
4	0.550	0.807	0.274	0.404	0.339	12
5	0.752	0.889	0.375	0.446	0.410	5
6	0.863	0.541	0.430	0.271	0.351	11
7	0.761	0.933	0.379	0.467	0.423	3
8	0.913	0.913	0.455	0.457	0.456	1
9	0.860	0.910	0.429	0.456	0.442	2
10	0.549	0.703	0.274	0.352	0.313	16
11	0.991	0.558	0.494	0.279	0.387	8
12	0.632	0.536	0.315	0.268	0.292	18
13	0.500	1.000	0.249	0.501	0.375	10
14	0.691	0.610	0.344	0.306	0.325	14
15	1.000	0.607	0.498	0.304	0.401	7
16	0.711	0.980	0.355	0.491	0.423	4
17	0.746	0.891	0.372	0.446	0.409	6
18	0.831	0.694	0.414	0.347	0.381	9

4.8. ANOVA for GRG

The GRG values are considered for ANOVA analysis, and calculated values are presented in Table 11. According to the table, EC contributes around 83% to machining performance. The next significant factor is DC which contributes 4.15% in the overall machining process. As per Table 12, the optimal combination is 28 g/l EC, 11 V MV, 85% DC and 37°C ET which is correlating with GRG ranking

Table 11
ANOVA for GRG

Symbol	DF	SS	MS	F	% Contribution
A	2	0.02995	0.01498	10.90	83.72
B	2	0.00080	0.00040	0.29	2.23
C	2	0.00148	0.00074	0.54	4.15
D	2	0.00080	0.00040	0.29	2.22
Error	9	0.01237	0.00137	1.00	7.68
Total	**17**	**0.04540**	**0.00267**	**13.02**	**100.00**

Table 12
Main effects table for GRG

Machining factors symbol	Mean values for GRG			
	L – I	L – II	L – III	Delta
EC	0.3231	0.3673	0.4228*	0.0997
MV	0.3661	0.3805*	0.3666	0.0143
DC	0.3667	0.3628	0.3837*	0.0170
ET	0.3651	0.3678	0.3803*	0.0027

*Optimal Combination using GRG: 28 g/l, 11 V, 85% and 37°

4.9. Comparison of TOPSIS, VIKOR and GRA

Figure 7 represents the overall optimized parameter combination for TOPSIS, VIKOR and GRA. As per the data available in the graph, the optimal combination using these three methods shows the same results for the experimental runs 8, 9 and 7. Hence the first rank merges with the 8th experimental run, and its parameter combination is 28 g/l EC, 11 V MV, 85% DC and 37°C ET. Hence this parameter combination is the best optimal

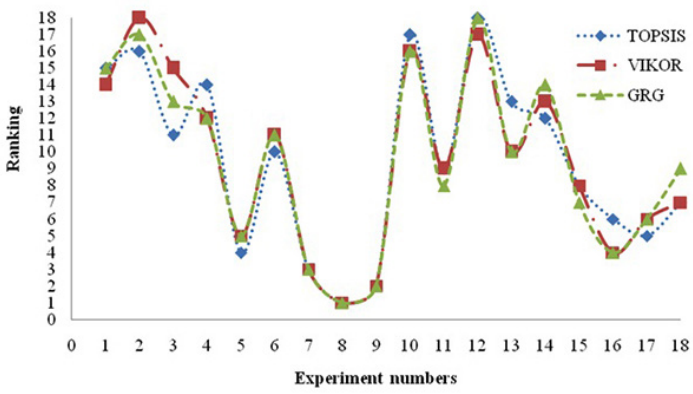

Fig. 7. Experimental Number Vs TOPSIS, VIKOR and GRA

combination to obtain the higher MR and lower OC. Furthermore, the 9th and 7th experimental runs are the next optimal combinations i.e. 28 g/l EC, 13 V MV, 75% DC, 37°C ET and 28 g/l EC, 9 V MV, 55% DC, 35°C ET, respectively.

5. CONCLUSIONS

The main objective of this study is to enhance the machining performance of ECMM using a magnetic field and UV heated electrolyte.The permanent magnet and UV rays were considered to increase the electrolyte temperature. L_{18} OA experimental design is used for conducting the experiments.The optimization technique such as TOPIS, VIKOR and GRA were considered to find the optimal parameter solution.

The MR increases consistently with an increase in input parameter levels.The highest and least MR are obtained at 13 V MV and 24 g/l EC, respectively.Moreover, the highest MR, i.e.0.733 µm/sec, is 35% higher than the previous studies. Weights of the responses (MR and OC) are determined using the Entropy weight method as 0.49872 and 0.50128, respectively.Based on the ANOVA results, the electrolyte concentration plays a major role, about 86% on machining performance. The second and least contributions are DC (3.86%) and ET (1.74%) respectively on the performance.The optimal combination using TOPSIS, VIKOR and GRA methods shows the same experimental combinations (experimental runs 8, 9 and 7) for optimal responses.The first optimal parameter solution is 28 g/l EC, 11 V MV, 85% DC and 37°C ET. Furthermore, the 9th and 7th experimental runs are next optimal combinations are 28 g/l EC, 13 V MV, 75% DC, 37°C ET and 28 g/l EC, 9 V MV, 55% DC, 35°C ET.The SEM images of micro holes for the 1st and 2nd optimal combination shows slight microcracks formations on the circumference of the micro holes due to the heat energy of the electrolyte.

REFERENCES

[1] X. Wu, L. Li, N. He, M. Zhao, and Z. Zhan, "Investigation on the influence of material microstructure on cutting force and bur formation in the micro cutting of copper," *Int. J. Adv. Manuf. Technol*., vol. 79, pp. 321–327, 2015, doi: 10.1007/s00170-015-6828-5.

[2] R. Thanigaivelan, R.M. Arunachalam, and P. Drukpa, "Drilling of micro-holes on copper using electrochemical micromachining," *Int. J. Adv. Manuf. Technol.* vol. 61, pp.1185–1190, 2012, doi: 10.1007/s00170-012-4093-4.

[3] S.S. Anasane and B. Bhattacharyya, "Electrochemical Micromachining of Titanium and Its Alloys," in *Non-traditional Micromachining Processes. Materials Forming, Machining and Tribology*, G. Kibria, B. Bhattacharyya, J. Davim, Eds., Springer, Cham, 2017, pp. 337–365, doi: 10.1007/978-3-319-52009-4_9.

[4] S. Min, D.-E. Lee, A. de Grave, C.M. De Oliveira Valente, J. Lin, and D.A. Dornfeld, "Surface and edge quality variation in precision machining of single crystal and polycrystalline materials," *Proc. Inst. Mech. Eng., Part B: J. Eng. Manuf.*, vol. 220, no. 4, pp. 479–487, 2006, doi: 10.1243/095440506X77599.

[5] M. Soundarrajan and R. Thanigaivelan, "Effect of coated geometrically modified tools on performance of electrochemical micromachining," *Mater. Manuf. Processes*, vol. 35, no. 7, pp. 775–782, 2020, doi: 10.1080/10426914.2020.1740252.

[6] T. Zhang, Z. Liu, and C. Xu, "Influence of size effect on burr formation in micro cutting," *Int. J. Adv. Manuf. Technol.* vol. 68, pp.1911–1917, 2013, doi: 10.1007/s00170-013-4801-8.

[7] S. Ao, K. Li, W. Liu, X. Qin, T. Wang, Y. Dai, and Z. Luo, "Electrochemical micromachining of NiTi shape memory alloy with ethylene glycol–NaCl electrolyte containing ethanol," *J. Manuf. Process*, vol. 53, pp. 223–228, 2020, doi: 10.1016/j.jmapro.2020.02.019.

[8] M. Soundarrajan, R. Thanigaivelan, and S. Maniraj, "Investigation on Electrochemical Micromachining (EMM) of AA-MMC Using Acidified Sodium Nitrate Electrolyte," in *Advances in Industrial Automation and Smart Manufacturing*, Springer 2019, pp. 367–376, doi: 10.1007/978-981-15-4739-3_30.

[9] K. Pooranachandran, J. Deepak, P. Hariharan, and B. Mouliprasanth, "Effect of Flushing on Electrochemical Micromachining of Copper and Inconel 718 Alloy," in *Advances in Industrial Automation and Smart Manufacturing*, Springer 2019, pp. 61–69, doi: 10.1007/978-981-13-1724-8_6.

[10] Y. Pan, Z. Hou, and N. Qu, "Improvement in accuracy of micro-dimple arrays prepared by micro-electrochemical machining with high-pressure hydrostatic electrolyte," *Int. J. Adv. Manuf. Technol.*, vol.100, no. 5, pp.1767–1777, 2019, doi: 10.1007/s00170-018-2822-z.

[11] M. Baoji, P. Cheng, K. Yun, and P. Yin, "Effect of magnetic field on the electrochemical machining localization," *Int. J. Adv. Manuf. Technol.*, vol. 102, no. 1–4, pp. 949–956, 2019, doi: 10.1007/s00170-018-3185-1.

[12] J. VinodKumaar, R. Thanigaivelan, and V. Dharmalingam, "A Study on the Effect of Oxalic Acid Electrolyte on Stainless Steel (316L) Through Electrochemical Micro-machining," in *Advances in Industrial Automation and Smart Manufacturing*, Springer 2019, pp. 93–103 2019, doi: 10.1007/978-981-32-9425-7_8.

[13] N. Rajan, R. Thanigaivelan, and K.G. Muthurajan, "Machinability studies on an A17075 composite with varying amounts of B_4C using an induction-heated electrolyte in electrochemical machining,"*Mater. Tehnol*., vol. 53, no. 6, pp. 873–880, 2019.

[14] R. Thanigaivelan, R.M. Arunachalam, M. Kumar, and B.P. Dheeraj, "Performance of electrochemical micromachining of copper through infrared heated electrolyte," *Mater. Manuf. Processes*, vol. 33, no. 4, pp. 383–389, 2018, doi: 10.1080/10426914.2017.1279304.

[15] K. Jiang *et al*., "Vibration-assisted wire electrochemical micromachining with a suspension of B_4C particles in the electrolyte," *Int. J. Adv. Manuf. Technol*., vol. 97, no. 9–12, pp. 3565–3574, 2018, doi: 10.1007/s00170-018-2190-8.

[16] W. Liu *et al*., "Electrochemical micromachining on titanium using the NaCl-containing ethylene glycol electrolyte," *J. Mater. Process. Technol.*, vol. 255, pp. 784–794, 2018, doi: 10.1016/j.jmatprotec.2018.01.009.

[17] A. Malik and A. Manna, "Investigation on the laser-assisted jet electrochemical machining process for improvement in machining performance," *Int. J. Adv. Manuf. Technol.*, vol. 96, no. 9–12, pp. 3917–3932, 2018, doi: 10.1007/s00170-018-1846-8.

[18] H. Zhang, S. Ao, W. Liu, Z. Luo, W. Niu, and K. Guo, "Electrochemical micro-machining of high aspect ratio micro-tools using quasi-solid electrolyte," *Int. J. Adv. Manuf. Technol.*, vol. 91, no. 9–12, pp. 2965–2973, 2017, doi: 10.1007/s00170-016-9900-x.

[19] A. Speidel, J. Mitchell-Smith, D.A. Walsh, M. Hirsch, and A. Clare, "Electrolyte jet machining of titanium alloys using novel electrolyte solutions," *Procedia CIRP*, vol. 42, pp. 367–372, 2016, doi: 10.1016/j.procir.2016.02.200.

[20] T. Sekar, M. Arularasu, and V. Sathiyamoorthy, "Investigations on the effects ofnano-fluid in ECM of die steel," *Measurement*, vol. 83, pp. 38–43. 2016, doi: 10.1016/j.measurement.2016.01.035.

[21] A. Mohanty, G. Talla, S. Dewangan, and S. Gangopadhyay, "Microstructural investigation and multi response optimization using Fuzzy-TOPSIS during the electrochemical machining of Inconel 825," *Int. J. Precis. Technol.*, vol. 5, pp. 201–216, 2015, doi: 10.1504/IJPTECH.2015.073825.

[22] D. Singh and R.S. Shukla, "Optimization of electrochemical micromachining and electrochemical discharge machining process parameters using firefly algorithm," *Int. J. Mechatron. Manuf. Syst*., vol. 9, pp.137–59, 2016, doi: 10.1504/IJMMS.2016.076169.

[23] A. Mehrvar, A. Basti, and A. Jamali, "Optimization of electrochemical machining process parameters: Combining response surface methodology and differential evolution algorithm," *Proc. Inst. Mech. Eng.*, *Part E: J. Process Mech. Eng.*, vol. 231, pp.1114–1126, 2017, doi: 10.1177/0954408916656387.

[24] O.V. Mythreyi, P. Hariharan, and S. Gowri, "Multi-objective optimization of electrochemical micro drilling of titanium alloy," *Int. J. Precis. Technol.*, vol. 7, pp.188–204, 2017, doi: 10.1504/IJPTECH.2017.090775.

[25] M. Soundarrajan and R. Thanigaivelan, "Investigation of Electrochemical Micromachining Process Using Ultrasonic Heated Electrolyte," in *Advances in Micro and Nano Manufacturing and Surface Engineering*, M. Shunmugam, M. Kanthababu, Eds., Springer, 2019, pp. 423–434, doi: 10.1007/978-981-32-9425-7_38.

[26] M. Soundarrajan and R. Thanigaivelan, "Investigation on electrochemical micromachining (ECMM) of copper inorganic material using UV heated electrolyte," *Russ. J. Appl. Chem.*, vol. 91, no. 11, pp. 1805–1813, 2018, doi: 10.1134/S1070427218110101.

[27] K. Motoyama, T. Umemoto, H. Shang, and T. Hasegawa "Effects of magnetic field and far-ultraviolet radiation on the structures of bright-rimmed clouds," *Astrophys. J.*, vol. 766, no 1, p. 50. 2013, doi: 10.1088/0004-637X/766/1/50.

[28] T. Mythili and R. Thanigaivelan, "Optimization of wire EDM process parameters on Al6061/Al_2O_3 composite and its surface integrity studies," *Bull. Pol. Acad. Sci. Tech. Sci*., vol. 68, no. 6, pp. 403–1412, 2020, doi: 10.24425/bpasts.2020.135382.

[29] J.R. Vinod Kumaar and R. Thanigaivelan, "Performance of magnetic field-assisted citric acid electrolyte on electrochemical micro-machining of SS 316L," *Mater. Manuf. Process*es, vol. 35, no. 9, pp. 969–977, 2020, doi: 10.1080/10426914.2020.1750630.